Journal of the Oceanographical Society of Japan
Vol. 46, pp. 55 to 67, 1990

A Steady Model of Typical Non-Large-Meander Paths of the Kuroshio Current*

Masaki Kawabe†

Abstract: Conditions south of Cape Shiono-misaki for the nearshore and offshore non-large-meander (NLM) paths of the Kuroshio Current are studied using a two-layer reduced gravity model. A steady and non-diffusive state is assumed, and the conservation laws of Bernoulli's function and potential vorticity along the current axis are used. Spatial changes of velocity and depth of the current are imposed as boundary conditions south of Cape Shiono-misaki. These conditions are based on the facts that are ohserved south of the cape: abrupt acceleration of the Kuroshio and the spatial change of sea levels. The current paths east of the cape are computed.

This model reproduces well the actual nearshore NLM paths. It also produces offshore NLM paths west of and over the Izu Ridge, but not east of the Izu Ridge. Diffusion of vorticity may be important for the eastern part of the offshore NLM path.

An increase of velocity south of the cape is necessary for producing realistic NLM paths. The velocity increase accompanies a decrease of current depth owing to Bernoulli's conservation, and the depth decrease in turn diminishes the absolute vorticity owing to the potential vorticity conservation. The velocity increase, on the other hand, strengthens the negative velocity shear and diminishes the relative vorticity. If the decreases of the relative and absolute vorticities compensate each other, the path goes excessively southward owing to the negative curvature south of the cape. Dominance of the relative vorticity change over the absolute vorticity change prevents the path from shifting southward and causes the realistic NLM paths.

The NLM paths need different amplitudes of the changes south of the cape depending on the velocity and transport of the current, but in any case, the nearshore NLM path needs larger changes than the offshore NLM path. This property and the amplitude of the changes are consistent with observations.

1. Introduction

The variation of the path of the Kuroshio Current south of Japan can be roughly described by three typical paths and the transitions between them (Kawabe, 1985, 1986). Figure 1 shows the typical paths: large-meander (LM) path and nearshore and offshore non-large-meander (NLM) paths. The LM path is located offshore, and the position is variable in time throughout the area between Kyûshû and the Izu Ridge (Taft, 1972; Kawabe, 1985). On the other hand, there is a clear difference of characteristics between the NLM paths west and east of Cape Shiono-misaki. They are always close to the coast west and south of the coape, while they leave the coast and become variable to the east. The classification of NLM paths into the nearshore and offshore paths is possible only in the eastern region of the cape (Kawabe, 1985).

A distinct difference is seen also between the surface velocities of the Kuroshio west and east of the cape during NLM periods. The mean velocity on the Kuroshio-current axis during the NLM period is much larger east of the Kii

* Received 19 May 1989; in revised form 23 February 1990; accepted 15 March 1990.

† Ocean Research Institute, University of Tokyo, Minamidai 1-15-1, Nakano-ku, Tokyo 164, Japan.

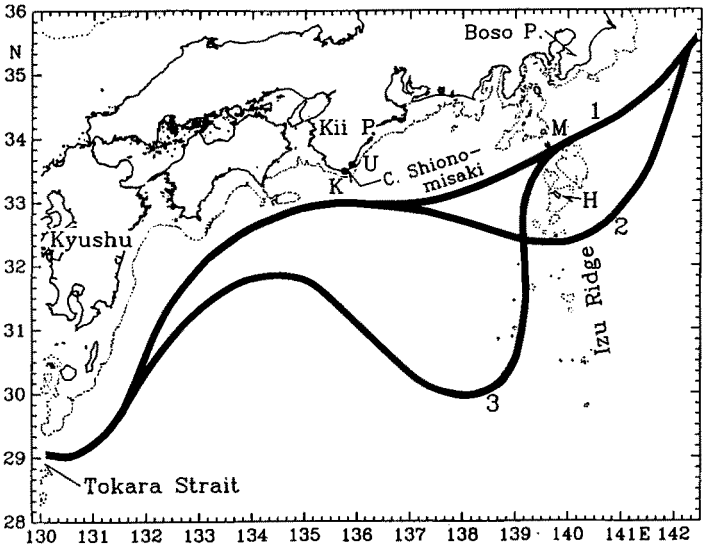

Fig. 1. Three typical paths of the Kuroshio south of Japan at mid-depth of about 500 m: 1. nearshore non-large-meander path, 2. offshore non-large-meander path, 3. typical large-meander path. *K* and *U* indicate tide stations at Kushimoto and Uragami. *M* and *H* are Miyake-jima and Hachijô-jima. Dotted lines show 500-m isobaths.

Peninsula than west (Masuzawa, 1961; Taft, 1972). The large increase of surface velocity of the Kuroshio occurs within a small region just south of Cape Shiono-misaki, according to the Kuroshio-tracking observations in May 1967, 1968 1970 and 1975 (Konaga *et al.*, 1967; Konaga, 1971; Minami, 1977; Shuto, 1979).

Moreover, there is a clear difference between the variations of coastal sea levels west of Kushimoto and east of Uragami during NLM periods (Tsumura, 1963; Kawabe, 1980). The sea-level difference between Kushimoto and Uragami, *i.e.*, the spatial change of sea level at the cape, correlates well with the alternate occurrences of nearshore and offshore NLM paths (Kawabe, 1989).

These facts suggest a strong connection between current conditions south of Cape Shiono-misaki and the NLM path east of the cape. The abrupt acceleration of the Kuroshio south of the cape may be important for the determination of the path east of the cape. The sea-level difference between Kushimoto and Uragami may be an important factor or, at least, its reflection.

In this paper, the effect of the spatial changes in the current velocity and depth on the NLM paths of the Kuroshio will be examined, using a simple steady model. The calculated paths, which do not pass through the two deep passages of the Izu Ridge, are considered impossible. This is because the nearshore and offshore NLM paths at mid-depth of about 500 m pass through the gap of the Izu Ridge between Miyake-jima and Hachijô-jima and through the deep region just south of Hachijô-jima, respectively (Kawabe, 1985). The conditions south of the cape which produce realistic paths will be discussed.

2. Model

As noted above, the NLM path of the Kuroshio leaves the coast in the eastern region of Cape Shiono-misaki, whereas it is close to the coast west of the cape. This suggests that the diffusion of vorticity east of the cape is less effective than that west of the cape where the vorticity of the Kuroshio may be diffused by the viscous coast, as in the numerical experiments by Yasuda *et al.* (1985). Yet, even in the area east of the cape, momentum and vorticity diffusion may not be neglected in the onshore region of the current axis owing to eddies advected from the coast west of the cape and coastal eddies formed in the eastern region. Therefore,

we will not think the onshore part of the Kuroshio and will consider only the Kuroshio current on the current axis (to be precise, just the offshore streamline of the axis) in the eastern area of the cape, and no diffusion of momentum and vorticity is assumed. A steady state is also assumed, since the nearshore and offshore NLM paths persist for several months. These assumptions lead to the conservation of Bernoulli's function and potential vorticity along the current axis.

A reduced gravity model is used; *i.e.*, the ocean is two-layered with a resting lower layer. The origin of the coordinates is taken at 135°40′E, 33°N just south of Cape Shiono-misaki, and the X-axis is taken eastward, the Y-axis northward, the x-axis downstream along the streamline of the current axis, and the y-axis perpendicular to the x-axis (Fig. 2).

Spatial changes of current depth and velocity are imposed at the origin as boundary conditions. These are based on observations of sea level and GEK velocity. The sea level at Uragami is lower than that at Kushimoto during the NLM period (Kawabe, 1980). This can be interpreted that the sea surface at the NLM path of the Kuroshio falls south of Cape Shiono-misaki, *i.e.*, at the origin of X-Y coordinates taken here. This implies that, in a two-layer reduced gravity model, the depth of the Kuroshio current decreases sharply south of the cape. The decrease of the depth on the current axis at the X-Y origin will be indicated by ΔH. The conservation of Bernoulli's function along the current axis is written as

$$\frac{1}{2}U_0^2+g'H_0=\frac{1}{2}U^2+g'(H_0-\Delta H), \qquad (1)$$

or

$$U=(U_0^2+2g'\Delta H)^{1/2}, \qquad (1)'$$

where U denotes the current velocity, H the depth of current (depth of the upper layer), and g' the reduced gravity. The quantities at the origin (to be more exact, just west of the origin) are indicated by the suffix 0.

Since the sea-level data imply $\Delta H>0$, Eq. (1)′ gives $U>U_0$; *i.e.*, the velocity on the current axis east of the origin is larger than that west. This agrees with the fact that the Kuroshio strongly accelerates just south of Cape Shiono-misaki.

The conservation of potential vorticity along the current axis is

$$\left(f_0-\frac{\partial u}{\partial y}_0+\kappa_0U_0\right)\cdot H_0^{-1}$$
$$=\left(f_0+\beta Y-\frac{\partial u}{\partial y}+\kappa U\right)\cdot(H_0-\Delta H)^{-1}\equiv C, \qquad (2)$$

where f is the Coriolis parameter, $\frac{\partial u}{\partial y}$ the horizontal shear of current velocity, and κ the curvature of the current path. The curvature κ is written as

$$\kappa=\frac{d^2Y}{dX^2}\cdot\left[1+\left(\frac{dY}{dX}\right)^2\right]^{-3/2}$$
$$=\frac{dP}{dX}\cdot(1+P^2)^{-3/2}, \qquad (3)$$

and

$$P=\frac{dY}{dX}, \qquad (4)$$

where $Y=Y(X)$ indicates the current axis on the $X-Y$ coordinates.

To estimate $\frac{\partial u}{\partial y}$ on thec urrent axis, the velocity profile needs to be assumed. Since the velocity of the Kuroshio decreases almost linearly in the offshore direction from the current axis, it is assumed as

$$u=\left(1+\frac{y}{L}\right)U, \qquad (5)$$

as shown in Fig. 2. The horizontal shear is

$$\frac{\partial u}{\partial y}=\frac{U}{L}, \qquad (6)$$

where L is the current width. Substitution of Eqs. (3) and (6) into Eq. (2) yields

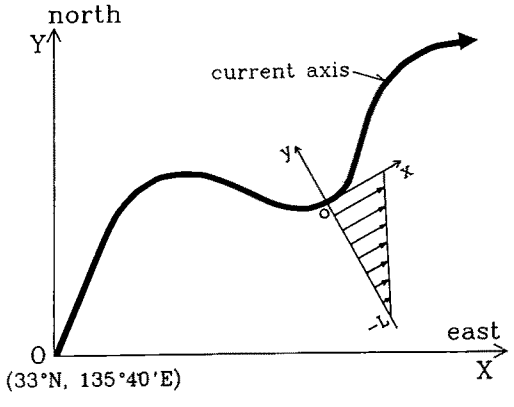

Fig. 2. Coordinates of the model. The origin of the X-Y coordinates is taken at 33°N, 135°40′E. Small arrows in the x-y coordinates show the assumed distribution of current velocity.

$$\frac{dP}{dX}+(\beta Y+C\,\Delta H+\frac{U_0}{L_0}-\frac{U}{L}-\kappa_0 U_0)\cdot U^{-1}\cdot(1+P^2)^{3/2}=0. \quad (7)$$

Equations (3), (4) and (7) are the equations for κ, P and Y. The values of f_0, β, g', κ_0 and H_0 are given as constants in Section (3), and U is calculated from Eq. (1)′ for given values of U_0 and ΔH. We can find a solution of Eqs. (3), (4) and (7), if L and L_0 are obtained.

By substituting Eq. (5) into the momentum equation $\kappa u^2+fu=-g'\frac{\partial h}{\partial y}$, the horizontal gradient of the current depth is given as

$$\frac{\partial h}{\partial y}=-\frac{\kappa U^2}{g'L^2}y^2-\frac{U}{g'L}(f+2\kappa U)y-\frac{U}{g'}(f+\kappa U).$$

If we neglect the y-dependence of κ, the current depth is approximately obtained as

$$h=-\frac{\kappa U^2}{3g'L^2}y^3-\frac{U}{2g'L}(f+2\kappa U)y^2-\frac{U}{g'}(f+\kappa U)y+H_0-\Delta H. \quad (8)$$

Using Eqs. (5) and (8), the volume transport $Q=\int_{-L}^{0}hu\cdot dy$ is given as

$$Q=U\left\{\left(\frac{\kappa U^2}{10g'}+\frac{fU}{8g'}\right)L^2+\frac{1}{2}(H_0-\Delta H)L\right\}. \quad (9)$$

In the same way, current depth and volume transport at the origin are obtained as

$$h_0=-\frac{\kappa_0 U_0^2}{3g'L_0^2}y^3-\frac{U_0}{2g'L_0}(f_0+2\kappa_0 U_0)y^2-\frac{U_0}{g'}(f_0+\kappa_0 U_0)y+H_0, \quad (10)$$

$$Q_0=U_0\left\{\left(\frac{\kappa_0 U_0^2}{10g'}+\frac{f_0 U_0}{8g'}\right)L_0^2+\frac{1}{2}H_0L_0\right\}. \quad (11)$$

Using Eqs. (9) and (11), the conservation of volume transport of the current, $Q=Q_0$, gives the equation of the current width L:

$$\left(\frac{\kappa U^2}{10g'}+\frac{fU}{8g'}\right)L^2+\frac{1}{2}(H_0-\Delta H)L=\frac{U_0}{U}\left\{\left(\frac{\kappa_0 U_0^2}{10g'}+\frac{f_0 U_0}{8g'}\right)L_0^2+\frac{1}{2}H_0L_0\right\}. \quad (12)$$

Moreover, Eq. (10) at $y=-L_0$ gives the equation of L_0 as

$$L_0=\frac{6g'}{U_0}\cdot\frac{D-H_0}{2\kappa_0 U_0+3f_0}, \quad (13)$$

where D is the depth of the upper layer on the offshore side of the current at the origin. Thus, L_0 is determined for a given value of D.

Finally, the unknowns κ, L, P, Y are numerically calculated through the following process, using Eqs. (3), (4), (7) and (12) for parameters U_0, ΔH and $P_0\left(=\frac{dY}{dX_0}\right.$: the inclination of current axis at the origin$\left.\right)$. [1] The position of the current axis Y at the n-th spatial step (written as Y_n hereafter) is computed from Eq. (4) using the known value of $P_{n-1}\left(=\frac{dY}{dX_{n-1}}\right)$. [2] P_n is similarly computed from the known value of $\frac{dP}{dX_{n-1}}$. [3] κ_n is computed from Eq. (3) using the value of P_n and the approximate value of $\frac{dP}{dX_n}$ given by $(P_n-P_{n-1})/\Delta X$. [4] L_n is computed from Eq. (12) using the value of κ_n. [5] $\frac{dP}{dX_n}$ is computed from Eq. (7) using the values of P_n, Y_n and L_n. [6] In order to obtain the final value of $\frac{dP}{dX_n}$, the processes [3] to [5] are repeated using the average between the approximate value in [3] and the computed value in [5] in terms of $\frac{dP}{dX_n}$, until the difference between the approximate and computed values becomes small. Then, P_{n+1} is computed from the final value of $\frac{dP}{dX_n}$ as in the process [2]. The values of P_n and P_{n+1} give the positions of the current axis Y_{n+1} and Y_{n+2}. The current path $Y=Y(X)$, thus, is obtained for a set of the parameters.

This model assumes that the velocity and depth of the current (accordingly, mass transport also) are constant along the current axis east of the coordinate origin. This implies $\frac{\partial v}{\partial y}=0$ on the current axis owing to the mass continuity, so that the current axis and its neighboring offshore streamline are parallel to each other. The requirement of parallel streamlines is implicitly extended to the whole current by the assumption of the triangle profile of velocity. Moreover, the y-dependency of streamline curvature is neglected in the derivation of Eq. (8). These assumptions

are satisfied when the current width is much smaller than the radius of streamline curvature, *i.e.*, $\kappa L \ll 1$. It should be noted that the present model is valid for currents with small curvature like non-large-meander paths of the Kuroshio.

3. Constants used in the model

The following values of constants are used: $f_0=0.8\times10^{-4}\,\mathrm{sec}^{-1}$, $\beta=1.9\times10^{-13}\,\mathrm{cm}^{-1}\,\mathrm{sec}^{-1}$, $g'=2\,\mathrm{cm\,sec}^{-2}$, $\kappa_0=-3\times10^{-8}\,\mathrm{cm}^{-1}$. The f_0 and β are the values at 33°N. The κ_0 is determined from the approximate curvature of the NLM path of the Kuroshio from south of Kyûshû to the Kii Peninsula.

The current depths H_0 and D are related to the volume transport Q_0 as

$$Q_0=\frac{g'}{2f_0}(D^2-H_0^2), \qquad (14)$$

if $\kappa_0=0$. The standard values of H_0 and D are specified as 500 m and 700 m, respectively. These values give the volume transport of $30\times10^6\,\mathrm{m}^3\,\mathrm{sec}^{-1}$, which is the approximate transport of the Kuroshio in the Tokara Strait estimated by the Hydrographic Department, Japan Maritime Safety Agency (Ishii *et al.*, 1986).

4. Effect of κ_0 and ΔH on the shape of current path

The small gradient case of the current axis, $\left(\frac{dY}{dX}\right)^2=P^2\ll1$, is discussed first, in order to survey the effects of the imposed condition at the origin on the shape of the current axis. Equation (7) is linearized to

$$\frac{d^2Y}{dX^2}=-\frac{\beta}{U}(Y+a), \qquad (15)$$

where

$$a=\beta^{-1}\left(C\Delta H+\frac{U_0}{L_0}-\frac{U}{L}-\kappa_0U_0\right). \qquad (16)$$

To be precise, the current width L depends on X and Y, since the first term in Eq. (12) involves κ and f. However, if we consider $f\gg\kappa U$ as well as $f\approx f_0$, L is treated as constant. With this approximation, the solution of Eq. (15) is

$$Y=A\cos\alpha X+B\sin\alpha X-a, \qquad (17)$$

where $\alpha=(\beta/U)^{1/2}$, and A and B are integral coefficients.

For the boundary conditions at the origin

$$Y=0,\quad \frac{dY}{dX}=P_0 \text{ at } X=0, \qquad (18)$$

it is concluded that

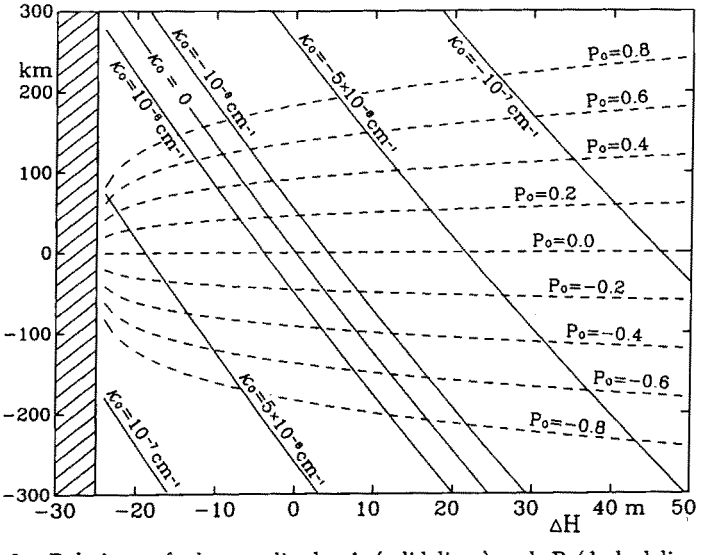

Fig. 3. Relations of the amplitude A (solid lines) and B (dashed lines) in Eq. (20) to the decrease of current depth at the origin, ΔH. The values of U_0, H_0 and D are 100 $\mathrm{cm\,sec}^{-1}$, 500 m and 700 m, respectively. The shaded area ($\Delta H<-25$ m) shows impossible cases with imaginary U.

$$A=a, \quad B=\alpha^{-1}P_0. \tag{19}$$

Finally, Eq. (17) can be written as

$$\begin{aligned} Y&=A(\cos\alpha X-1)+B\sin\alpha X \\ &=a(\cos\alpha X-1)+\alpha^{-1}P_0\sin\alpha X. \end{aligned} \tag{20}$$

This indicates that the mean meridional position of the current axis shifts to $Y=-A$. The quantity A is proportional to κ_0 and U_0 if $\Delta H=0$, and is strongly influenced by the other terms in Eq. (16) as ΔH increases. The amplitude of the sine term, B, is proportional to the inclination of the current axis at the origin, P_0.

If the values of H_0, D and U_0 are given as constant, the coefficient A depends on κ_0 and ΔH, and B depends on P_0 and ΔH, *i.e.*, $A=A$ (κ_0, ΔH) and $B=B$ (P_0, ΔH). These relations are shown in Fig. 3. The coefficient A depends strongly on both κ_0 and ΔH, while B depends on P_0 but not strongly on ΔH (especially for large ΔH). Therefore, the current path for given P_0 is almost entirely determined by κ_0 and ΔH, and there are innumerable pairs of κ_0 and ΔH giving similar paths. For example, a pair of (κ_0, ΔH) $=(-10^{-8}\,\mathrm{cm^{-1}}$, 15 m) and ($-5\times10^{-8}\,\mathrm{cm^{-1}}$, 36 m)

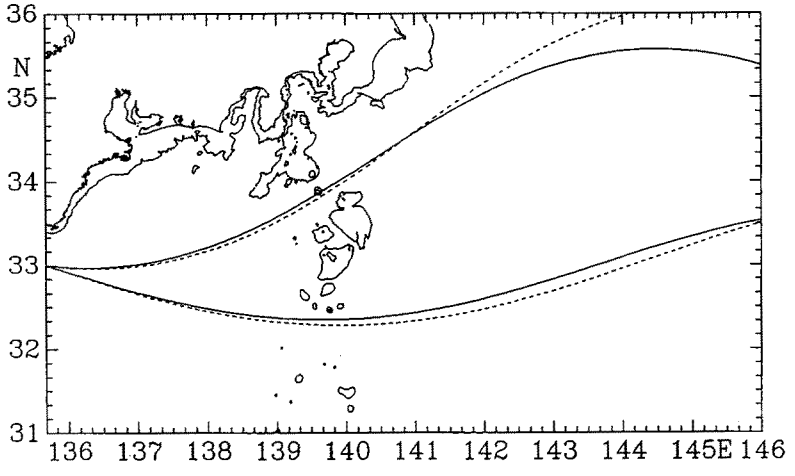

Fig. 4. Computed current paths for the following values of P_0, κ_0, and ΔH: -0.1, $-10^{-8}\,\mathrm{cm^{-1}}$, 15 m (upper solid), -0.1, $-5\times10^{-8}\,\mathrm{cm^{-1}}$, 36 m (upper dashed), -0.3, $-10^{-8}\,\mathrm{cm^{-1}}$, 4 m (lower solid) and -0.3, $-5\times10^{-8}\,\mathrm{cm^{-1}}$, 22 m (lower dashed). U_0, H_0 and D are 100 cm sec^{-1}, 500 m and 700 m, respectively. The 500-m isobaths are shown together with the coast lines.

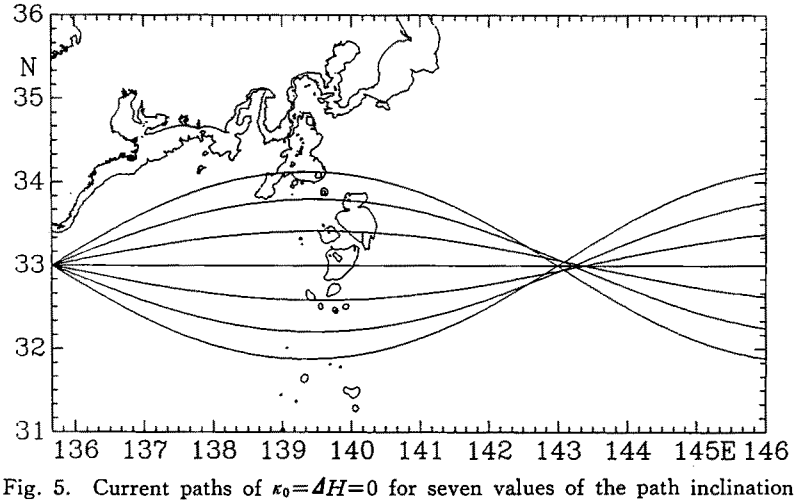

Fig. 5. Current paths of $\kappa_0=\Delta H=0$ for seven values of the path inclination at the origin, P_0. The values of P_0 are -0.6, -0.4, -0.2, 0, 0.2, 0.4, 0.6. U_0, H_0 and D are 100 cm sec^{-1}, 500 m and 700 m, respectively.

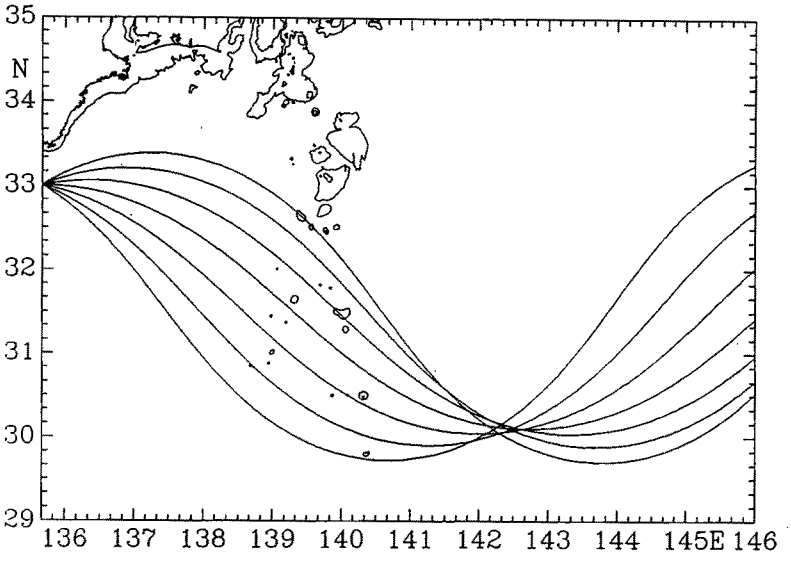

Fig. 6. Same as Fig. 5 except for $\kappa_0 = -3 \times 10^{-8}$ cm^{-1}.

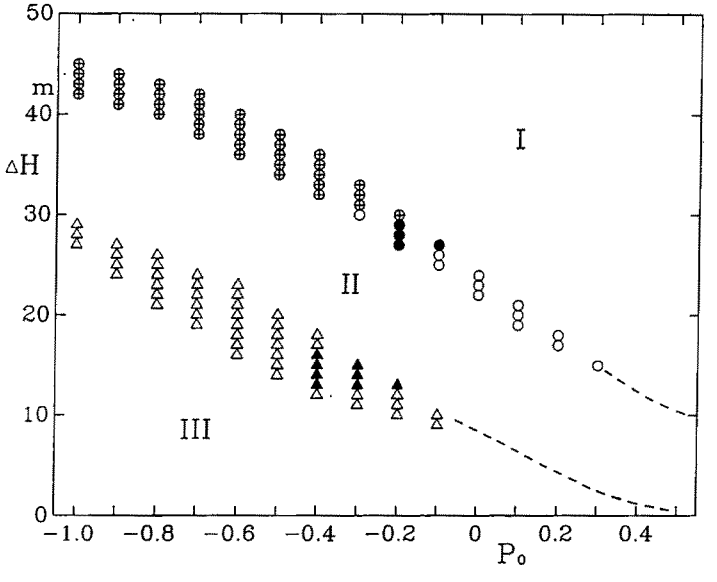

Fig. 7. Classification of paths for values of ΔH and P_0 ($U_0 = 100$ cm sec^{-1}, $H_0 = 500$ m, $D = 700$ m, $\kappa_0 = -3 \times 10^{-8}$ cm^{-1}). The regions I and II show the paths which collide with the Izu Ridge shallower than 500 m at the north and south of Miyake-jima, respectively. The mark ⊕ shows the path which collides with the coastal slope off the Bôsô Peninsula after passing through the gap of the Izu Ridge between Miyake-jima and Hachijô-jima. Circles show the paths passing through the gap of the Izu Ridge. Triangles are the paths which pass through the deep area south of Hachijô-jima and do not reach to 32°N. Paths in the region III are unreal because they reach 32°N. Solid circles and solid triangles show realistic paths of the nearshore and offshore NLM paths, respectively (see the text for the criterion of realistic paths).

for $P_0=-0.1$ and another pair of $(\kappa_0,\ \Delta H)=(-10^{-8}\,\mathrm{cm}^{-1},\ 4\,\mathrm{m})$ and $(-5\times10^{-8}\,\mathrm{cm}^{-1},\ 22\,\mathrm{m})$ for $P_0=-0.3$ give similar current paths, respectively (Fig. 4). (Note that Figs. 4, 5 and 6 are drawn by the procedure mentioned in Section 2.) The effect of κ_0 on the current path can almost be replaced by that of ΔH.

When both the parameters κ_0 and ΔH are zero, the current for $P_0=0$ flows directly eastward from the origin, and the currents for non-zero P_0 take sine-like paths, as expected from the linear discussion (Fig. 5). The contribution of P^2 in Eq. (7) can be seen in the difference of the points crossing $Y=0$. When κ_0 is not zero, the path for $\Delta H=P_0=0$ is similar to $\cos\alpha X-1$ (Fig. 6). A sine-like component as in Fig. 5 is added to it by non-zero P_0.

Figure 6 shows that the Kuroshio path goes too far southward owing to its negative curvature at the origin if $\Delta H=0$ (*i.e.*, $U=U_0$). The current depth and velocity need to be changed at the origin in order to obtain realistic paths of the Kuroshio.

5. Conditions at the origin for realistic paths

Figure 7 shows a classification of paths for values of ΔH and P_0. The paths in the regions I and II collide with the Izu Ridge which is shallower than 500 m. The paths shown by ⊕ pass through the gap of the Izu Ridge between Miyake-jima and Hachijô-jima, but thereafter collide with the coastal slope off the Bôsô Peninsula. The other paths do not collide with the bottom topography. Parts of them pass through the gap of the Izu Ridge (circles), and the others pass through the deep area south of Hachijô-jima (triangles and region III). The region III produces unreal paths which reach to the south of 32°N. Therefore, parts of the circles and triangles are expected to show the conditions which produce realistic nearshore and offshore NLM paths, respectively.

The criterion of the realistic paths needs to be determined here. On the basis of the mid-depth paths of the Kuroshio shown in Kawabe (1985), it is decided that the nearshore NLM path must be located between 142°20′E and 143°30′E at 36°N, and that the offshore NLM path must take a southernmost position between 139°E and 140°E. Moreover, values of P_0 are assumed to be more than -0.4, *i.e.*, $P_0>-0.4$, since the NLM path at the south and just east of Cape Shiono-misaki is directed almost eastward. The paths which satisfy these requirements are shown in Fig. 8, and the corresponding conditions are indicated by solid marks in Fig. 7.

The nearshore NLM paths are reproduced very well, despite the use of a simple model (Fig. 8). They are very similar to the real paths at mid-depth. On the other hand, the offshore NLM paths east of the Izu Ridge do not resemble the real paths, though they are realistic west of and over the Izu Ridge. The offshore NLM path in the real ocean goes northward in the region east of the Izu Ridge and is located at nearly the same position as the nearshore NLM

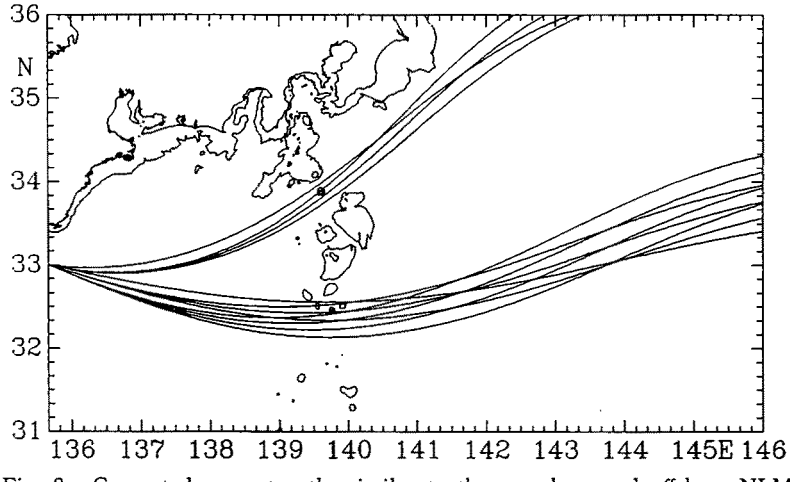

Fig. 8. Computed current paths similar to the nearshore and offshore NLM paths. They correspond to the solid circles and triangles in Fig. 7.

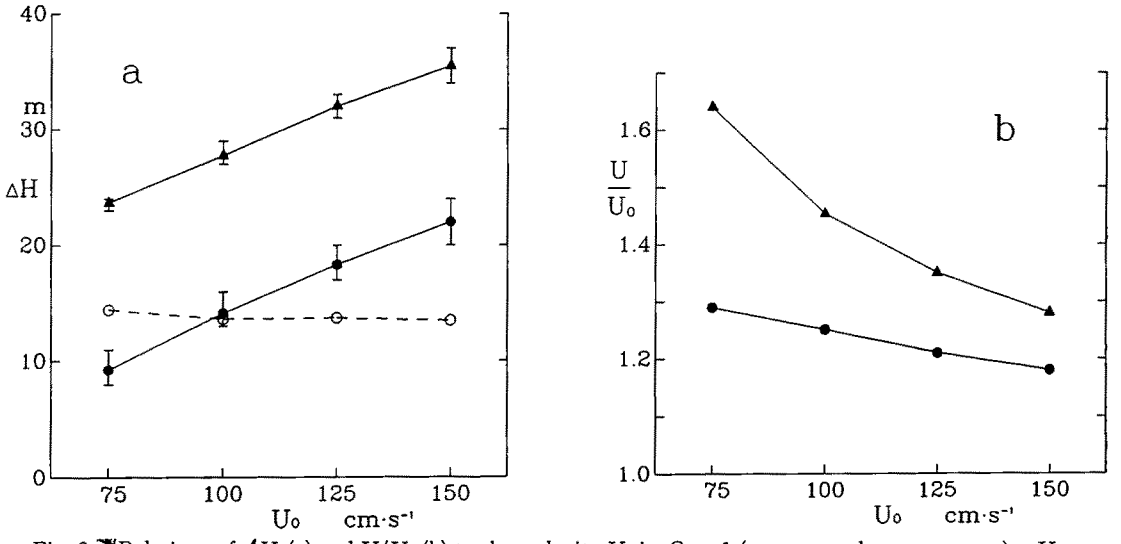

Fig. 9. Relations of ΔH (a) and U/U_0 (b) to the velocity U_0 in Case 1 (constant volume transport). H_0= 500 m, D=700 m, $\kappa_0=-3\times10^{-8}$ cm^{-1}. Solid triangles and circles are for the nearshore and offshore NLM paths, respectively. Open circles with dashed lines in Fig. 9a show the difference of ΔH between the nearshore and offshore NLM paths. Vertical bars in Fig. 9a indicate the ranges of ΔH that produce the NLM paths.

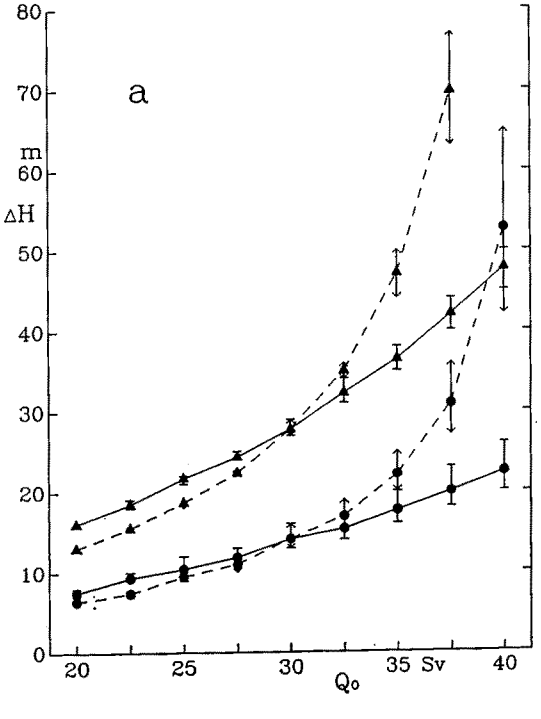

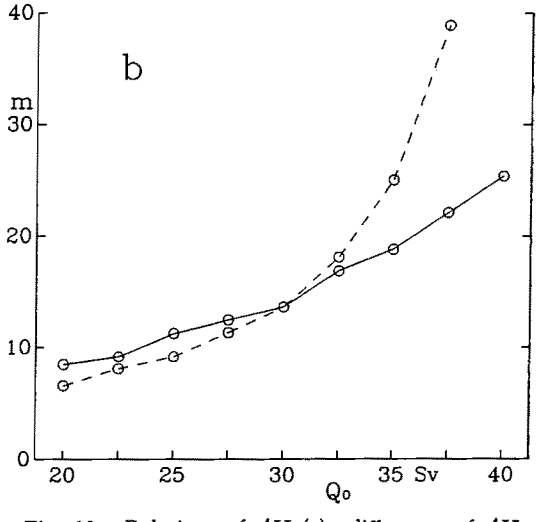

Fig. 10. Relations of ΔH (a), difference of ΔH between the NLM paths (b), and U/U_0 (c) to the volume transport Q_0 in C ase 2 (constant velocity). U_0=100 cm sec^{-1}, $\kappa_0=-3\times10^{-8}$ cm^{-1}. Solid lines show the cases with constant H_0 (=500 m) in which the volume transport is changed by D, and dashed lines are the cases with constant D(=700 m) where the transport is changed by H_0. Solid triangles and circles are for the nearshore and offshore NLM paths, respectively. Vertical bars in Fig. 10a indicate the ranges of ΔH which produce the NLM paths.

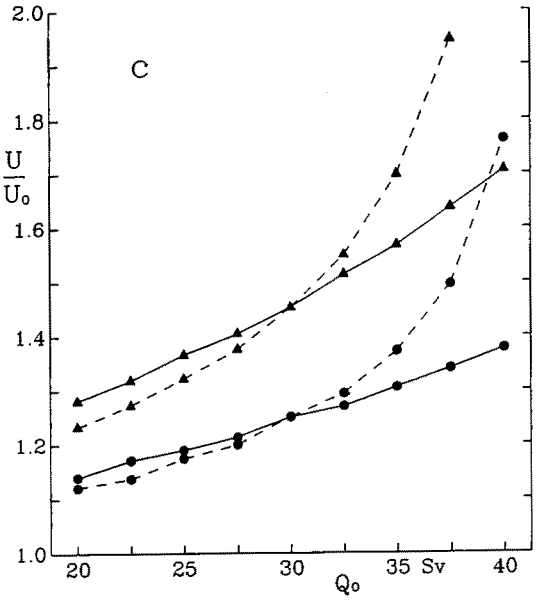

Fig. 10c

path to the east of the Bôsô Peninsula. In order to reproduce such a large northward component of the flow east of the Izu Ridge, the path inclination at the origin P_0 must be -0.8 or less in this model. However, such nearly southeastward flow at the origin is not realistic. The offshore NLM path east of the Izu Ridge cannot be reproduced by a model in which no eastern boundary condition exists and the potential vorticity and energy are conserved along the streamline. The Kuroshio actually may have to pass east of the Bôsô Peninsula under the restriction by the large ocean circulation, and the vorticity may be diffused significantly in the offshore NLM path east of the Izu Ridge.

6. Dependence of conditions at the origin on velocity and volume transport of the current

In this section, dependence of the conditions at the origin on velocity and volume transport for the NLM paths will be examined in terms of the current-depth change ΔH, the difference in ΔH between the nearshore and offshore NLM paths, and the velocity ratio U/U_0. Figure 9 shows the dependence of the quantities on velocity

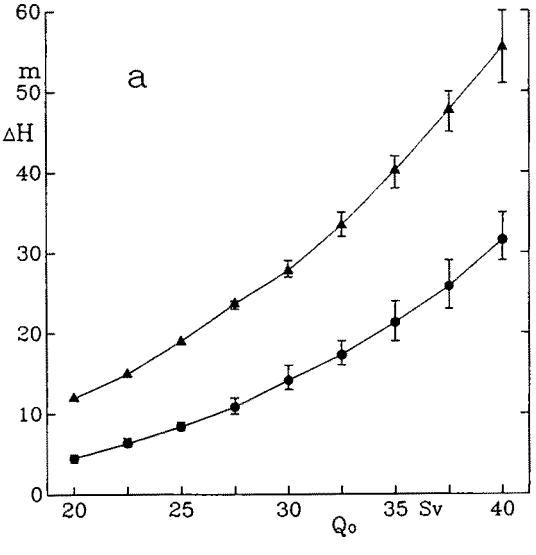

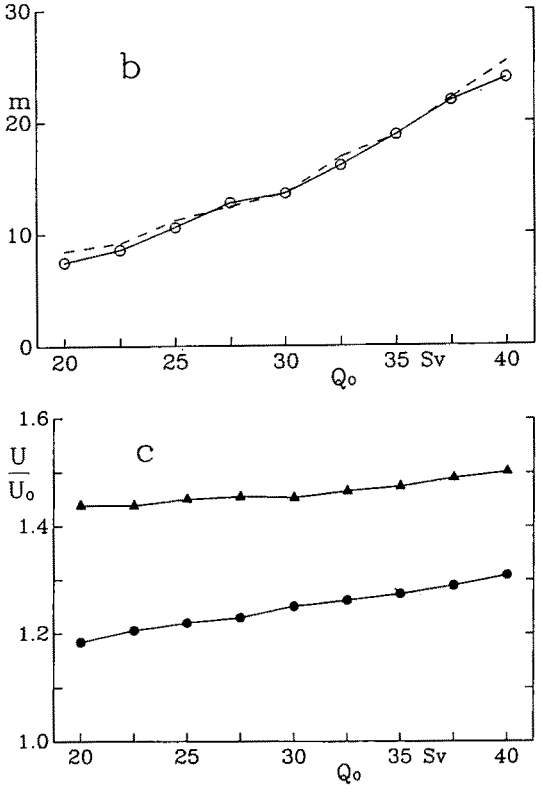

Fig. 11. Same as Fig. 10 except for Case 3 (Q_0 and U_0 are proportional to each other. $U_0=100$ cm sec^{-1} for $Q_0=30\times10^6$ m^3 sec^{-1}). The value of H_0 is constant (=500 m), and the volume transport is changed by D. The solid line in Fig. 10b is shown by the dashed line in Fig. 11b for comparison.

for the constant volume transport of 30×10^6 m^3 sec^{-1} ($H_0=500$ m, $D=700$ m): the transport-fixed case (called Case 1 hereafter). Figure 10 shows their dependence on volume transport for the constant velocity of 100 cm sec^{-1}: the velocity-fixed case (Case 2). The volume transport is changed by D (solid line) and by H_0 (dashed line). Figure 11 shows the dependence on the velocity and volume transport which are proportional to each other (Case 3). The value of H_0 is fixed at 500 m, and the transport is changed by D. Case 3 is considered realistic, because the volume transport of the Kuroshio actually tends to correlate with the velocity (Nitani, 1975). The case of $U_0=100$ cm sec^{-1} and $Q_0=30\times10^6$ m^3 sec^{-1} ($H_0=500$ m, $D=700$ m) is shown commonly in all the cases as standard.

The change of current depth at the origin, ΔH, is always larger for the nearshore NLM path than for the offshore NLM path (Figs. 9a, 10a and 11a). The magnitude is enhanced as velocity or volume transport increases. The value of ΔH in Case 3 is larger at $Q_0>30\times10^6$ m^3 sec^{-1} (*i.e.*, $U_0>100$ cm sec^{-1}) and smaller at $Q_0<30\times10^6$ m^3 sec^{-1} ($U_0<100$ cm sec^{-1}) than that in Case 2 ($U_0=100$ cm sec^{-1}) (Fig. 11a). This can be understood from the property that ΔH increases with velocity when the volume transport is fixed.

The difference in ΔH between the nearshore and offshore NLM paths increases with transport (Fig. 10b), but it does not change with velocity if the transport is fixed (Fig. 9a). Therefore, the difference in ΔH in Cases 2 and 3 increases similarly with transport (Fig. 11b).

The ratio of velocity in the downstream area to that at the origin, U/U_0, is always larger for the nearshore NLM path than for the offshore NLM path in all the cases, as in the case with ΔH. However, unlike ΔH, its dependency on velocity is opposite to that on transport. The velocity ratio increases greatly with transport as in ΔH (Fig. 10c), whereas it decreases with an increase of the velocity U_0, especially for the nearshore NLM path (Fig. 9b). Therefore, in Case 3, the effects of velocity and transport compensate each other, and the velocity ratio increases only slightly (Fig. 11c).

In Case 2, all of the quantities (ΔH, the difference in ΔH between the paths, and U/U_0) increase with transport, and the rate of increase is larger in the D-fixed case than in the H_0-fixed case (Fig. 10). The current is more sensitive to the change of H_0 than to that of D, probably because H_0 contributes to the potential vorticity on the current axis.

7. Conclusion and discussion

Conditions south of Cape Shiono-misaki for non-large-meander (NLM) paths of the Kuroshio Current are examined in terms of spatial change of current velocity and depth of the Kuroshio. The model is steady, non-diffusive, two-layered with a resting lower layer, and is based on the conservation of Bernoulli's function and potential vorticity along the current axis.

If any quantity of the current does not change, the path goes excessively southward east of the cape owing to its negative curvature south of the cape. The spatial change of a current quantity is needed to reproduce a realistic NLM path. On the basis of GEK and sea-level observations, the abrupt changes of current velocity and depth are imposed at the coordinate origin, which is taken just south of Cape Shiono-misaki in the present model. Consequently, realistic NLM paths that pass through the deep passages in the Izu Ridge are obtained. The spatial changes of current velocity and depth in the region south of the cape are necessary for the NLM paths of the Kuroshio to have realistic location and shape.

An increase of the current velocity south of Cape Shiono-misaki brings about a decrease of current depth and current width through the conservation of Bernoulli's function and volume transport, respectively. The increase of the current velocity as well as the decrease of the current width enhance the horizontal shear of velocity U/L and diminish the relative vorticity south of the cape (U is the velocity on the current axis, and L the current width). On the other hand, the decrease of current depth diminishes the absolute vorticity $f+\kappa U-U/L$ so as to conserve the potential vorticity (f is the Coriolis parameter, and κ the curvature of the current axis). If the decreases of absolute and relative vorticities compensate each other, $f+\kappa U$ is conserved, and the paths similar to those in Fig. 6 are obtained. The effect of $-U/L$ must exceed that of the current depth in order to reproduce realistic NLM paths; the surplus of the $-U/L$ effect causes the path to have larger

Coriolis parameter owing to the conservation of potential vorticity, and the mean position of the path shifts northward east of Cape Shiono-misaki. The change in horizontal shear of velocity south of the cape is very important for reproducing realistic NLM paths in this model.

The present model produces nearshore NLM paths very well, while it produces offshore NLM paths west of and over the Izu Ridge fairly well. However, as long as a moderate inclination of the path is assumed at the origin, it cannot produce the offshore NLM path east of the Izu Ridge that runs northward to the Bôsô Peninsula. Diffusion of vorticity may be needed for the eastern part of the offshore NLM path.

The ratio (U/U_0) of current-axis velocity (U_0 and U are velocities at the origin and in the downstream area, respectively) as well as the decrease (ΔH) of current depth at the origin must be larger for the nearshore NLM path than for the offshore NLM path. The nearshore NLM path needs greater changes south of Cape Shiono-misaki than the offshore NLM path.

The velocity ratio U/U_0 around the Kii Peninsula can be estimated by GEK data which are thought to be taken near the Kuroshio-current axis. Six observations from 1967 to 1975 indicate that the values during the nearshore NLM path are 1.44 on the average with a range between 1.25 and 1.71, while five observations from 1965 to 1971 indicate that the values during the offshore NLM path are 1.24 on the average with a range between 1.1 and 1.36. These mean values correspond to the values of the ratio at transports of $23\times10^3\,m^3\,sec^{-1}$ and $29\times10^6\,m^3\,sec^{-1}$ in Fig. 11c. On the other hand, the current-depth change ΔH can be compared with the sea-level difference between Kushimoto and Uragami by assuming that the sea levels roughly show the surface height at the Kuroshio-current axis. The sea-level difference of Kushimoto minus Uragami during the nearshore NLM path is larger by 3.7 cm than that during the offshore NLM path (Kawabe, 1989). This implies that ΔH during the nearshore NLM path is larger by 18.1 m than that during the offshore NLM path. Figure 11b shows this value at the transport of $34.5\times10^6\,m^3\,sec^{-1}$. Thus, the observational data agree with the model results that U/U_0 and ΔH for the nearshore NLM path are larger than those for the offshore NLM path. They show also that the present model gives reasonable values of U/U_0 and of the difference of ΔH between the paths. These points suggest that the results of this model are valid.

Acknowledgement

This work was completed at the College of Marine Studies, University of Delaware, USA. I wish to express my gratitude to Dr. Ferris Webster and his group for their kind help.

Maps in the figures were drawn using the JODC file of isobath data (No. 84-037 for JODC reference).

References

Ishii, H., Y. Michida and H. Nishida (1986): Estimation of Kuroshio volume transport from ADCP data. Report of the Kuroshio Exploitation and Utilization Research (KER), No. 9, 167-180.

Kawabe, M. (1980): Sea level variations along the south coast of Japan and the large meander in the Kuroshio. J. Oceanogr. Soc. Japan, **36**, 97-104.

Kawabe, M. (1985): Sea level variations at the Izu Islands and typical stable paths of the Kuroshio. J. Oceanogr. Soc. Japan, **41**, 307-326.

Kawabe, M. (1986): Transition processes between the three typical paths of the Kuroshio. J. Oceanogr. Soc. Japan, **42**, 174-191.

Kawabe, M. (1989): Sea level changes south of Japan associated with the non-large-meander path of the Kuroshio. J. Oceanogr. Soc. Japan, **45**, 181-189.

Konaga, S. (1971): On the relation between Kuroshio strong current and water temperature of 200 m depth III. Umi to Sora, **46**, 77-85 (in Japanese with English abstract and legends).

Konaga, S., K. Shuto, H. Kusano and K. Hori (1967): On the relation between Kuroshio strong currents and the water temperature of 200 m depth (II). Umi to Sora, 43, 48-53 (in Japanese with English abstract and legends).

Masuzawa, J. (1961): Recent research on the Kuroshio current. Geogr. studies presented to Prof. Tsujimura in honor of his 70th birthday, 354-364 (in Japanese with English abstract).

Minami, H. (1977): Sudden increase of the Kuroshio surface current off Shionomisaki and the role of the southward flow off Kumano-nada. Umi to Sora, **53**, 15-22 (in Japanese with English abstract and legends).

Nitani, H. (1975): Variation of the Kuroshio south of Japan. J. Oceanogr. Soc. Japan, **31**, 154-173.

Shuto, K. (1979): The flow conditions of the Kuroshio in the vicinity of Cape Shionomisaki. Oceanogr. Mag., **30**, 1-14.

Taft, B. (1972): Characteristics of the flow of the Kuroshio south of Japan. p. 165-216. *In*: Kuroshio—Its physical aspects, ed. by H. Stommel and K. Yoshida, Univ. Tokyo Press, Tokyo.

Tsumura, K. (1963): Investigation of the mean sea level and its variation along the coast of Japan (Part I)—Regional distribution of sea level variation. J. Geodetic Soc. Japan, **9**, 49-90 (in Japanese with English abstract and legends).

Yasuda, I., J.-H. Yoon and N. Suginohara (1985): Dynamics of the Kuroshio large meander—Barotropic model. J. Oceanogr. Soc. Japan, **41**, 259-273.

黒潮の非大蛇行接岸・離岸流路の定常モデル

川　辺　正　樹*

要旨　下層を静止させた2層モデルを使い，黒潮の非大蛇行流路の再現に必要な潮岬南での条件を調べた．非粘性定常状態を仮定し，流軸に沿ってのベルヌーイ関数とポテンシャル渦度の保存則を用いた．流速と流れの厚さが潮岬南で空間的に急変するという境界条件のもとに，潮岬から東側の流路を求めた．この条件は潮岬南での観測事実，黒潮の急激な加速と沿岸潮位の低下をモデル化したものである．

その結果，現実に非常に近い非大蛇行接岸流路が得られた．一方，非大蛇行離岸流路は伊豆海嶺上および西側では現実に近いものの，東側では異なる。海嶺東側の離岸流路では，実際には渦度の粘性消散が効いているものと思われる．

非大蛇行流路の再現には，潮岬南での流速の増加が必要である．流速の増加はベルヌーイの保存則によって流れの厚さの減少を伴い，厚さの減少はポテンシャル渦度の保存則によって絶対渦度を減少させる．一方，流速の増加は負の流速シアを強化して相対渦度を減少させる．もしこれらの渦度変化が相殺すれば，上流側流路の負の曲率の影響で流路は極端に南偏したものとなる．相対渦度の減少が絶対渦度の減少を上回ることで，流路の南偏が抑えられ，現実的な非大蛇行流路が実現される．

流路の実現に必要な潮岬南での変化の大きさは流速や流量の大きさによって異なるものの，どの場合でも接岸流路の方が離岸流路よりも大きな変化を必要とする．この性質および変化の大きさは，観測事実とよく一致する．

* 東京大学海洋研究所
〒164 東京都中野区南台1-15-1